Comprehensive Analysis and Design of a Pulsating Signal Injection-based Position Observer for Sensorless Synchronous Motor Drives

L. Ortombina, *Member*, *IEEE*, D. Pasqualotto, F. Tinazzi, *Member*, *IEEE*, and M. Zigliotto, *Senior Member*, *IEEE*

***Abstract*—The work focuses on a new mathematical formulation for the transfer function of a pulsating injection-based position observer, as the key point for its correct design. The proposed analysis exploits the modulation/demodulation control theory to derive the transfer function of the whole estimator in the Laplace domain. Magnetic iron saturation effects and cross–saturation between the dq-axes are taken into consideration in the observer design. To test the effectiveness of the new transfer function representation of the observer, it is used to synthesise two different regulators, namely by the direct synthesis and the internal model principle. An extensive experimental stage is included pointing to fully verify the accuracy of the proposed model and the theoretical considerations. A comparison with the existing mathematical model of the observer is also reported to show the improvement achievable in the position estimation by the proposed observer synthesis.**

***Index Terms*—sensorless, position observer, interior permanent magnet (IPM), synchronous reluctance, high-frequency injection**

I. Introduction

In the recent times, sensorless motor drives have obtained considerable attention from both academy and industry seeking higher system reliability, reduced equipment price and a shrunk motor frame. Several sensorless techniques have been proposed so far, which can mainly be bundled in two groups according to the operating motor speed. In medium–high speed range, position observers based on fundamental frequency signals are implemented, such as those based on the extended back–electromotive force (BEMF) or the active flux [1], [2]. At standstill and low speed working region, the estimation of fundamental frequency signals is troublesome or, worst, impossible. However, the rotor position can be estimated by injecting high frequency (HF) voltages superimposed to the fundamental components and looking at the induced HF currents, provided that the rotor anisotropy is detectable [3], [4]. Interior Permanent Magnet (IPM) and Synchronous Reluctance (SynR) motors are notably suitable for the HF rotor position estimation thanks to their pronounced rotor anisotropy.

The paper has never been presented at conference or submitted previously.
L. Ortombina is with the Department of Industrial Engineering, University of Padova, 35131 Padova, Italy (e-mail:ludovico.ortombina@unipd.it)
D. Pasqualotto, F. Tinazzi, and M. Zigliotto are with the Department of Management and Engineering, University of Padova, 36100 Vicenza, Italy (e-mail: dario.pasqualotto@studenti.unipd.it; fabio.tinazzi@unipd.it; mauro.zigliotto@unipd.it) *Corresponding author: Ludovico Ortombina.*

HF injection methods can be classified according to the reference frame in which signals are injected, namely the stator or the estimated reference frame synchronous to the rotor. Methods of the former group adopt HF voltage signals superimposed to the fundamental frequency in the stator reference frame [5], thus the name of *rotating signal injection* sensorless techniques. The rotor position is retrieved by demodulating the negative–sequence carrier current through a synchronous reference frame filter. A recent advance of this technique is reported in [6], where the rotor position is obtained by taking advantage of the HF currents which describe an ellipse in the stator reference frame. The information about the rotor position is nested in the major axis tilt, thus a fitted model of the ellipse is adopted and updated online. However, the rotating injected signal induces a detrimental torque ripple and the rotor position estimation suffers from an injection frequency-dependent position estimation error [7]. The flaws of the rotating signal injection techniques can be overcome, or partially weakened, by the methods of the latter group. A HF voltage signal is injected in one of the estimated synchronous reference frame axis, usually the d–axis [3], [4], [8]. The rotor position is recovered through the minimisation of the measured pulsating current along the estimated q–axis, which is obtained by means of an observer.

Synchronous motor drives performances rely on accurate rotor electric position information. Whatever reason that may undermine the accuracy of the rotor position should be carefully addressed. In case of pulsating signal injection-based sensorless drives, the adopted estimator performance and accuracy mainly depend on its regulator, which goal is to nullify a variable of interest, i.e. the pulsating current along the estimated q–axis. In a sensorless motor drive, several outer control loops interact with each other, which results in a very complex design process. In fact, the controllers poles allocation must be carried out carefully to guarantee stability and satisfactory system performances at the same time [9]. Model–based design methods allow to guarantee excellent performances provided that the model of the plant is accurate.

So far, the literature about pulsating injection sensorless techniques report a plant description obtained by blending together both time and Laplace–domain expressions [3], [5], [8], neglecting the transfer function frequency shifting due to the modulation/demodulation process. The ensuing plant description is not accurate and the regulator cannot be properly

tuned, resulting in detrimental effects on the position estimation accuracy.

In this paper, the pulsating injection sensorless plant is modelled by exploiting the modulation/demodulation theory [10]. The whole system is described in the Laplace domain, including the effects of the modulation/demodulation process on dynamic blocks like filters. The differences between the proposed analysis of the sensorless technique and the classical one are in-depth analysed and discussed. Furthermore, the resulting transfer function is exploited to design two regulators with different design methodologies, namely the direct synthesis and the internal model principle.

For the sake of completeness, magnetic saturations and cross–coupling are considered. Indeed, their effects on sensorless motor drive are twofold: they trouble the regulator dynamic by altering the static gain of the plant and they undermine the observer stability. The former issue is considered since the transfer function is involved, whereas the latter is outlined, but no compensation is proposed since it does not fall within the scope of this article. The stability issue and remedies are described in [3], [4], whereas [11] demodulates the pulsating *q*–flux to assure zero tracking error.

The paper is organised as follows. The theoretical background of the pulsating injection sensorless technique is described in Section II. The proposed transfer function is thoroughly explained in Section III. An exhaustive discussion about the position observer design by means of two different regulator design methods are described in Section IV. A complete set of experimental tests is reported in Section V, accompanied by an in-depth discussion of the results.

II. Theoretical background

The voltage balance equations of a synchronous motor in the *dq* rotating reference frame fixed to the rotor are:

$$\begin{aligned} u_d &= R_s i_d + \frac{d\lambda_d(i_d,i_q)}{dt} - \omega_{\text{me}}\lambda_q(i_d,i_q) \\ u_q &= R_s i_q + \frac{d\lambda_q(i_d,i_q)}{dt} + \omega_{\text{me}}\lambda_d(i_d,i_q) \end{aligned} \tag{1}$$

where u_d, u_q are the stator voltages, i_d, i_q are the stator currents, λ_d and λ_q are the flux linkages and $\omega_{\text{me}} = p\omega_{\text{m}}$ are electric speed, pole pairs and mechanical speed, respectively. It is worth highlighting the explicit dependence of the flux linkages on the *dq* currents in (1). Finally, the possible presence of permanent magnet (PM) flux linkage Λ_{mg} is included in $\lambda_d(i_d,i_q)$.

The currents-to-flux linkage relationships are usually nonlinear due to magnetic saturation. By linearising the flux linkages and expanding the derivative terms by means of the chain rule, yields:

$$\begin{aligned} \frac{d\lambda_d(i_d,i_q)}{dt} &= L_{dd}(i_d,i_q)\frac{di_d}{dt} + L_{dq}(i_d,i_q)\frac{di_q}{dt} \\ \frac{d\lambda_q(i_d,i_q)}{dt} &= L_{dq}(i_d,i_q)\frac{di_d}{dt} + L_{qq}(i_d,i_q)\frac{di_q}{dt} \end{aligned} \tag{2}$$

where L_{dd} and L_{qq} are the self-differential inductances and L_{dq} is the cross-differential inductance. Still, the differential inductances depend on the operating point as much as the flux linkages in (1). To ease the mathematical notation, the explicit dependence from stator currents will be omitted from now on.

A. Pulsating injection-based position estimator analysis

The pulsating injection sensorless technique estimates the rotor position by injecting a high frequency sinusoidal voltage signal along the estimated $\hat{d}$–axis superimposed to the voltage reference generated by the current controller, i.e.:

$$\widehat{u}_{h,d} = U_h \cos(\omega_h t) \tag{3}$$

where U_h and ω_h are the magnitude and the pulsation frequency of the injected sine wave. The hat superscript highlights the variables obtained in the estimated rotor reference frame. Let $\widetilde{\vartheta}_{\text{me}} = \widehat{\vartheta}_{\text{me}} - \vartheta_{\text{me}}$ be the estimation error between the estimated electrical rotor position $\widehat{\vartheta}_{\text{me}}$ and the actual one ϑ_{me}. The high frequency currents induced by the voltage injection are:

$$\begin{aligned} \widehat{i}_{h,d} &= M\left[L_\Sigma - L_\Delta\cos(2\widetilde{\vartheta}_{\text{me}}) - L_{dq}\sin(2\widetilde{\vartheta}_{\text{me}})\right]\sin(\omega_h t) \\ \widehat{i}_{h,q} &= M\left[L_\Delta\sin(2\widetilde{\vartheta}_{\text{me}}) - L_{dq}\cos(2\widetilde{\vartheta}_{\text{me}})\right]\sin(\omega_h t) \end{aligned} \tag{4}$$

where $L_\Sigma \triangleq (L_{dd}+L_{qq})/2$, $L_\Delta \triangleq (L_{dd}-L_{qq})/2$ and $M \triangleq U_h/(\omega_h(L_{dd}L_{qq}-L_{dq}^2))$. At the injection frequency, the resistive voltage drop is negligible with respect to the inductive one, whereas the motional voltage terms are disregarded due to the low operating speed. The $\widehat{i}_{h,q}$ current can be exploited to obtain the rotor position, as sketched in Figure 1.

At first, neglecting the cross–differential inductances contribution in (4) and rearranging the expression of $\widehat{i}_{h,q}$ yields:

$$\widehat{i}_{h,q} = \frac{U_h L_\Delta}{\omega_h L_{dd} L_{qq}}\sin(2\widetilde{\vartheta}_{\text{me}})\sin(\omega_h t) = I_{h,q}\sin(\omega_h t) \tag{5}$$

where $I_{h,q} = \frac{U_h L_\Delta}{\omega_h L_{dd} L_{qq}}\sin(2\widetilde{\vartheta}_{\text{me}})$. The rotor position information can be extracted from $\widehat{i}_{h,q}$ by using the demodulation scheme shown in Figure 1 [8], [9]. A high pass filter is used to extract the alternating component $\widehat{i}_{h,q}$ from i_q. To demodulate the high frequency q-current, the filtered signal is then multiplied with a sinusoidal wave as follows:

$$\widehat{i}_{h,q}\sin(\omega_h t) = I_{h,q}\sin^2(\omega_h t) = \frac{I_{h,q}}{2}\left[1-\cos(2\omega_h t)\right]. \tag{6}$$

A low pass filter is applied to block the component at twice the perturbation frequency in (6). Assuming a small estimation error, the demodulated signal amplitude can be further approximated as:

$$\frac{I_{h,q}}{2} = \frac{U_h L_\Delta}{2\omega_h L_{dd} L_{qq}}\sin(2\widetilde{\vartheta}_{\text{me}}) \approx \frac{U_h L_\Delta}{\omega_h L_{dd} L_{qq}}\widetilde{\vartheta}_{\text{me}}. \tag{7}$$

Finally, steering the demodulated signal to zero by means of an observer, the rotor position is estimated and it can be exploited for the motor control. It is worth noting that the estimator performances rely on the observer tuning. Therefore an accurate plant modelling by means of a transfer function (TF) is crucial.

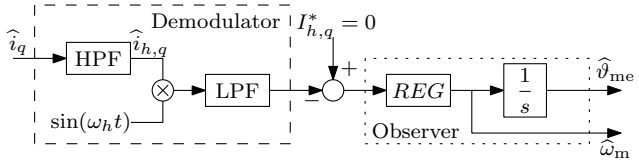

Fig. 1: The considered position observer.

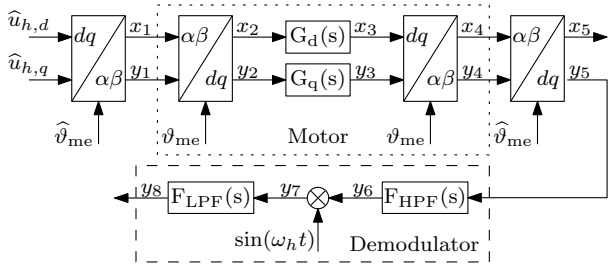

Fig. 2: Computation of the observer transfer function.

III. Estimator transfer function analysis

A. The existing mathematical approach

The achievable control performances of a sensorless drive deeply depend on the estimator ones and, in turn, on that of the observer regulator. The observer TF $P_{\rm obs}^{\rm past}$ is adopted to carry out model-based design techniques, and it is usually derived in time domain as in Section II-A. In particular, combining (7) with the low-pass and the high-pass filter used in the demodulator, one obtains:

$$P_{\rm obs}^{\rm past}(\mathrm{s}) = \frac{I_{h,q}(\mathrm{s})}{\widehat{\vartheta}_{\rm me}(\mathrm{s})} = \frac{U_h L_\Delta}{\omega_h L_{dd} L_{qq}} F_{\rm LPF}(\mathrm{s}) F_{\rm HPF}(\mathrm{s}). \quad (8)$$

As inferable from Figure 1, one can note that (8) indiscriminately combines time– and Laplace–domain based quantities, which is not formally correct. In the conventional approach, the high–pass filter removes the fundamental component from i_q, but the resulting translation in the frequency domain is completely disregarded. In this way, the design based on that model leads to wrong stability analysis and inaccurate bandwidth, both critical in sensorless control design.

B. The proposed improved approach

A proper approach to derive the estimator TF can be accomplished by observing that each Park's transformation consists in a modulation/demodulation at the actual or estimated electrical position in addition to the real demodulation in the estimator, i.e. equation (5). This method was used in [12] to derive the TF of a current injection-based technique for the stator resistance estimation. All the modulation/demodulation blocks of the position estimator with pulsating injection are sketched in Figure 2. $G_{\rm d}(\mathrm{s})$ and $G_{\rm q}(\mathrm{s})$ stand for the electrical motor dynamics, and the motional terms are neglected due to the low motor speed. For the sake of simplicity, the cross–differential inductances are initially neglected, but they will be considered in Section III-C.

An approximated transfer function for a modulated and demodulated system of a particular form was derived in [10]. The Laplace transform of a generic modulated signal $\varsigma(t) = \cos(\omega_d t + \phi)x(t)$ is:

$$\mathcal{L}(\varsigma) = \frac{\left[e^{j\phi}X(\mathrm{s} - j\omega_d) + e^{-j\phi}X(\mathrm{s} + i\omega_d)\right]}{2} \quad (9)$$

where $\mathcal{L}$ is the Laplace operator and $X(\mathrm{s})$ is the Laplace transform of the signal $x(t)$. The (9) can be effectively exploited to obtain a TF of the modulated system $y(t) = \cos(\omega_d t) \times G(\mathrm{s}) \times \cos(\omega_d t + \phi)$ depicted in Figure 3, where $\times$ stands for the modulation process. It is worth noting that $y(t)$ includes all the elements that assembles a position estimator, namely sine[1] and cosine modulation/demodulation at generic pulsation frequency ω_d, as well as a dynamic filtering $G(\mathrm{s})$. According to (9), the TF of the modulated input $u_{\rm m}(t)$ is:

$$U_{\rm m}(\mathrm{s}) = \frac{[U(\mathrm{s} - j\omega_d) + U(\mathrm{s} + j\omega_d)]}{2}. \quad (10)$$

The modulated signal is then filtered by $G(\mathrm{s})$, which yields:

$$Y_{\rm m}(\mathrm{s}) = G(\mathrm{s})U_{\rm m}(\mathrm{s}). \quad (11)$$

The (9) can be further applied to obtain the Laplace transform of the demodulated output, yielding:

$$Y(\mathrm{s}) = \frac{\left[e^{j\phi}Y_{\rm m}(\mathrm{s} - j\omega_d) + e^{-j\phi}Y_{\rm m}(\mathrm{s} + j\omega_d)\right]}{2}. \quad (12)$$

Expanding the equation (12) by using (10) and (11), the Laplace transform of the demodulated output becomes:

$$\begin{aligned} Y(\mathrm{s}) = {} & \frac{\left[e^{-j\phi}G(\mathrm{s} - j\omega_d) + e^{j\phi}G(\mathrm{s} + j\omega_d)\right]}{4}U(\mathrm{s}) + \\ & \frac{e^{j\phi}G(\mathrm{s} - 2j\omega_d)U(\mathrm{s} - 2j\omega_d)}{4} + \\ & \frac{e^{-j\phi}G(\mathrm{s} + j\omega_d)U(\mathrm{s} + 2j\omega_d)}{4}. \end{aligned} \quad (13)$$

Then, it is possible to conclude that the original modulated system $y(t) = \cos(\omega_d t) \times G(\mathrm{s}) \times \cos(\omega_d t + \phi)$ can be represented in Laplace domain by (13).

A similar procedure can be adopted to obtain the baseband approximation of the whole pulsating injection sensorless plant, with any other combination of modulated and demodulation carriers. Assuming $\vartheta_{\rm me} = \omega_{\rm me} t$, $\widehat{\vartheta}_{\rm me} = \widehat{\omega}_{\rm me} t$ and $\widetilde{\omega}_{\rm me} = \widehat{\omega}_{\rm me} - \omega_{\rm me}$, it follows that the Laplace transform of signals $x_3(t)$ and $y_3(t)$ in Figure 2 is:

$$\begin{aligned} X_3(\mathrm{s}) = {} & \frac{G_{\rm d}(\mathrm{s})}{2}\Big[U_{\rm d}(\mathrm{s} + j\widetilde{\omega}_{\rm me}) + U_{\rm d}(\mathrm{s} - j\widetilde{\omega}_{\rm me}) \dots \\ & - jU_{\rm q}(s + j\widetilde{\omega}_{\rm me}) + jU_{\rm q}(s - j\widetilde{\omega}_{\rm me})\Big] \\ Y_3(\mathrm{s}) = {} & \frac{G_{\rm q}(\mathrm{s})}{2}\Big[jU_{\rm d}(\mathrm{s} + j\widetilde{\omega}_{\rm me}) - jU_{\rm d}(\mathrm{s} - j\widetilde{\omega}_{\rm me}) \dots \\ & + U_{\rm q}(s + j\widetilde{\omega}_{\rm me}) + U_{\rm q}(s - j\widetilde{\omega}_{\rm me})\Big] \end{aligned} \quad (14)$$

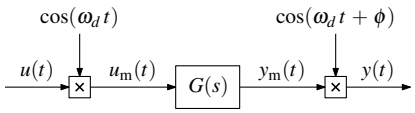

Fig. 3: Modulated system.

[1] $\cos(\omega_d t + \pi/2) = -\sin(\omega_d t)$

and that of signals $x_5(t)$ and $y_5(t)$ is:

$$\begin{aligned} X_5(\mathrm{s}) &= \frac{1}{2}\Big[X_3(\mathrm{s}+j\widetilde{\omega}_{\mathrm{me}}) + X_3(\mathrm{s}-j\widetilde{\omega}_{\mathrm{me}})\ldots \\ &\quad + jY_3(s+j\widetilde{\omega}_{\mathrm{me}}) - jY_3(s-j\widetilde{\omega}_{\mathrm{me}})\Big] \\ Y_5(\mathrm{s}) &= \frac{1}{2}\Big[-jX_3(\mathrm{s}+j\widetilde{\omega}_{\mathrm{me}}) + jX_3(\mathrm{s}-j\widetilde{\omega}_{\mathrm{me}})\ldots \\ &\quad + Y_3(s+j\widetilde{\omega}_{\mathrm{me}}) + Y_3(s-j\widetilde{\omega}_{\mathrm{me}})\Big] \end{aligned} \tag{15}$$

where $U_{\mathrm{d}}(\mathrm{s})$ and $U_{\mathrm{q}}(\mathrm{s})$ are the Laplace transforms of the high frequency injected signals $\widehat{u}_{h,d}(t)$ and $\widehat{u}_{h,q}(t)$, respectively.

The demodulation process is the most critical element of the observer. With a slight abuse of notation, the demodulated signal can be written as $y_8(t) = F_{\mathrm{LPF}}(\mathrm{s})\left[(F_{\mathrm{HPF}}(\mathrm{s})y_5(t)) \times \sin(\omega_h t)\right]$, then its Laplace transform is:

$$\begin{aligned} Y_8(\mathrm{s}) = \frac{jF_{\mathrm{LPF}}(\mathrm{s})}{2}\Big[&F_{\mathrm{HPF}}(\mathrm{s}+j\omega_h)Y_5(\mathrm{s}+j\omega_h)\ldots \\ &-F_{\mathrm{HPF}}(\mathrm{s}-j\omega_h)Y_5(\mathrm{s}-j\omega_h)\Big]. \end{aligned} \tag{16}$$

Expression (16) can be expanded by using (14) and (15), and remembering that the Laplace transform of the injected signal (3) is $U_{\mathrm{d}}(\mathrm{s}) = U_h\mathrm{s}/(\mathrm{s}^2+\omega_h^2)$ while $U_{\mathrm{q}}(\mathrm{s}) = 0$, the approximated estimator TF is:

$$I_{h,q}(\mathrm{s}) = \frac{L_\Delta U_h}{L_{dd}L_{qq}\omega_h}F^{\Sigma}_{\mathrm{HPF}}(s)F_{\mathrm{LPF}}(\mathrm{s})(\widehat{\vartheta}_{\mathrm{me}}(\mathrm{s}) - \vartheta_{\mathrm{me}}(\mathrm{s})) \tag{17}$$

where:

$$F^{\Sigma}_{\mathrm{HPF}}(\mathrm{s}) = \frac{1}{2}\left(F_{\mathrm{HPF}}(\mathrm{s}+j\omega_h) + F_{\mathrm{HPF}}(\mathrm{s}-j\omega_h)\right). \tag{18}$$

See the Appendix for the proof.

The new estimator TF is:

$$P^{\mathrm{new}}_{\mathrm{obs}}(\mathrm{s}) = \frac{I_{h,q}(\mathrm{s})}{\widehat{\vartheta}_{\mathrm{me}}(\mathrm{s})} = \frac{U_h L_\Delta}{\omega_h L_{dd}L_{qq}}F_{\mathrm{LPF}}(\mathrm{s})F^{\Sigma}_{\mathrm{HPF}}(\mathrm{s}) \tag{19}$$

which differs from the classic expression (8), both for the generalised static gain, i.e. the function gain without zeros and/or poles in the origin, and for the frequency behaviour. It is worth reminding that motor inductances are still dependent from stator currents, thus static gain of (8) and (19) varies as a function of the operating point. Figure 4 depicts the frequency response of $F^{\Sigma}_{\mathrm{HPF}}(\mathrm{s})$ and $F_{\mathrm{HPF}}(\mathrm{s})$ obtained with the parameters utilised in this paper and reported in Table II. It is worth noting that $F^{\Sigma}_{\mathrm{HPF}}(\mathrm{s})$ is akin to a (weak) notch filter at the injection pulsation ω_h with a non unitary generalised static gain $F^{\Sigma}_{\mathrm{HPF}}(0) = \omega_h^2/(\omega_h^2+\omega_{\mathrm{H}}^2)$. The sag depth is bounded from below to -6dB with respect to the static gain when the cut-off frequency of the high pass filter is lower enough respect to the injection one.

The observer static gain of (19) differs from the one in (8) for the factor $F^{\Sigma}_{\mathrm{HPF}}(0)$ which, however, tends to 1 in the above condition, i.e. when the cut-off frequency of the high pass filter is lower enough respect to the injection one. Thus, the gain mismatch between (8) and (19) is almost negligible. These considerations allow to draw the conclusion that the two observer TF, with a proper HPF cut-off frequency, have the same generalised static gain and high-frequency behaviour, while they differ in the low frequency range. Finally, it is worth remembering that $F^{\Sigma}_{\mathrm{HPF}}(\mathrm{s})$ is the Laplace description of $F_{\mathrm{HPF}}(\mathrm{s})$ used in a control scheme with a modulation/demodulation process. The discretisation of $F_{\mathrm{HPF}}(\mathrm{s})$ is implemented in the estimator, whereas $F^{\Sigma}_{\mathrm{HPF}}(\mathrm{s})$ is used to design the estimator regulator.

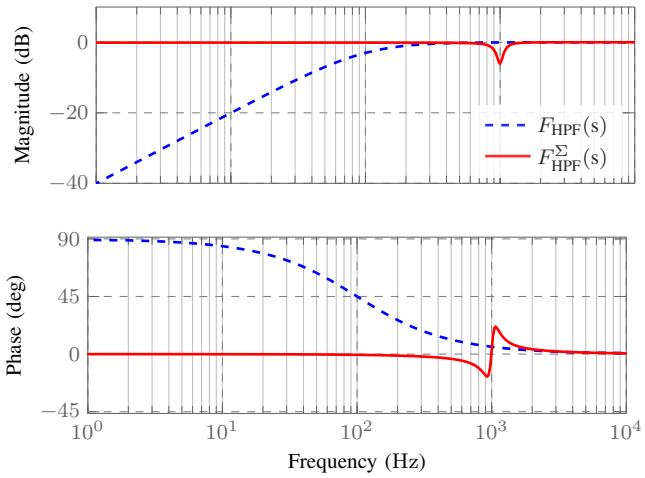

Fig. 4: Transfer function of the conventional high–pass filter $F_{\mathrm{HPF}}(\mathrm{s})$ and the new representation $F^{\Sigma}_{\mathrm{HPF}}(\mathrm{s})$.

C. Cross–Inductances Effects

The high frequency q-current in (4) is rearranged as:

$$\widehat{i}_{h,q} = \frac{U_h\sqrt{L_\Delta^2 + L_{dq}^2}}{\omega_h(L_{dd}L_{qq} - L_{dq}^2)}\sin(2\widetilde{\vartheta}_{\mathrm{me}} + 2\bar{\vartheta})\sin(\omega_h t) \tag{20}$$

where $\bar{\vartheta} \triangleq 0.5\,\mathrm{atan2}(-L_{dq}, L_\Delta)$. In order to obtain the rotor position estimation, the $\widehat{i}_{h,q}$ is demodulated by means of the technique described in Section II-A. The output of the demodulation process is steered to zero through an observer.

Actually, the stable point of the observer is $\widetilde{\vartheta}_{\mathrm{me}} = -\bar{\vartheta}$, that is the solution of the demodulated high frequency current. It is worth highlighting that $\bar{\vartheta} \neq 0$ if $L_{dq} \neq 0$, thus the observer is unable to perfectly track the rotor position due to the non–zero cross–differential inductances. Furthermore, the position estimation error induced by the cross-inductances could lead to stability issues in the observer [3] for highly saturated machines. Despite this, its effects and its compensation overcomes the purpose of this paper which focuses on an accurate description of the observer and the TF of the plant at high frequencies.

The existing observer TF including the cross differential inductances can be obtained by combining (20) with the low-pass and the high-pass filter, as in (8), i.e.:

$$P^{\mathrm{past}}_{\mathrm{obs}}(\mathrm{s}) = \frac{U_h\sqrt{L_\Delta^2 + L_{dq}^2}}{\omega_h(L_{dd}L_{qq} - L_{dq}^2)}F_{\mathrm{LPF}}(\mathrm{s})F_{\mathrm{HPF}}(\mathrm{s}) \tag{21}$$

where only the static gain changes due to cross-inductances. However, the same observation about the arbitrary combination of time– and frequency–domain quantities reported in (8) applies to (21). In order to derive the estimator TF with the proposed method based on the modulation/demodulation

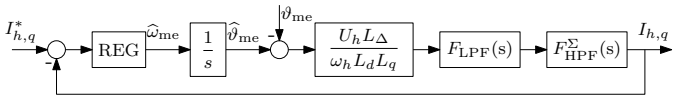

Fig. 5: Observer control loop of a pulsating sensorless drive.

theory, it is enough to remember that signals $x_3(\mathrm{s})$ and $y_3(\mathrm{s})$ in Figure 2 are:

$$\begin{aligned} X_3(\mathrm{s}) &= G_{\mathrm{d}}(\mathrm{s})X_2(\mathrm{s}) + G_{\mathrm{dq}}(\mathrm{s})Y_2(\mathrm{s}) \\ Y_3(\mathrm{s}) &= G_{\mathrm{dq}}(\mathrm{s})X_2(\mathrm{s}) + G_{\mathrm{q}}(\mathrm{s})Y_2(\mathrm{s}) \end{aligned} \tag{22}$$

but $G_{\mathrm{d}}(\mathrm{s}) = L_{qq}/[(L_{dd}L_{qq} - L_{dq}^2)\mathrm{s}]$, $G_{\mathrm{q}}(\mathrm{s}) = L_{dd}/[(L_{dd}L_{qq} - L_{dq}^2)\mathrm{s}]$ and $G_{\mathrm{dq}}(\mathrm{s}) = -L_{dq}/[(L_{dd}L_{qq} - L_{dq}^2)\mathrm{s}]$ are now considered. Following the procedure described in Section III, the demodulated q-axis current Laplace transform is:

$$I_{h,q}(\mathrm{s}) = \frac{U_h\sqrt{L_\Delta^2 + L_{dq}^2}}{\omega_h(L_{dd}L_{qq} - L_{dq}^2)} F^{\Sigma}_{\mathrm{HPF}}(s)F_{\mathrm{LPF}}(\mathrm{s})(\widetilde{\vartheta}_{\mathrm{me}}(\mathrm{s}) + \bar{\vartheta}(\mathrm{s})) \tag{23}$$

and the observer TF is:

$$P^{\mathrm{new}}_{\mathrm{obs}}(\mathrm{s}) = \frac{I_{h,q}(\mathrm{s})}{\widehat{\vartheta}_{\mathrm{me}}(\mathrm{s})} = \frac{U_h\sqrt{L_\Delta^2 + L_{dq}^2}}{\omega_h(L_{dd}L_{qq} - L_{dq}^2)} F_{\mathrm{LPF}}(\mathrm{s})F^{\Sigma}_{\mathrm{HPF}}(\mathrm{s}) \tag{24}$$

which is akin to (19), except for the static gain which takes into account no zero cross–differential inductances.

IV. Observer Regulator Design

A sensorless drive is composed by four closed control loops, namely the observer loop, the dq-current loops and the speed one. The observer controller requirements are twofold, i.e. a wide and well–known closed–loop bandwidth and a high disturbance rejection capability. In particular, the former allows to boost the position tracking capability during transients and it may improve the latter. Moreover, the observer loop interacts with the other control loops [9]. Therefore, the actual design of the real bandwidth is crucial to guarantee the whole motor drive stability and performance.

The observer scheme is reported in Figure 5, where the actual position acts as a disturbance with detrimental effects on control performances. In other words, the disturbance rejection capability of the observer is critical. Finally, the (19) is considered in Figure 5 for simplicity, since the only difference with (24) is the different static gain.

In this paper, the direct synthesis (DS) method, which allows an accurate closed–loop bandwidth supervision, and the internal model principle with the Bode's synthesis, which can design an effective controller against a disturbance, are analysed. Finally, the DS is used to verify the proposed observer model (19) correctness against the classical one (8).

A. Direct Synthesis Tuning

Direct synthesis method is based upon prescribing a desired form for the system's response and then finding a controller strategy and parameters to give that response. It is able to take into account systems with a non unitary feedback. Let $R(\mathrm{s})$, $P(\mathrm{s})$ and $F(\mathrm{s})$ be the TFs of the regulator, the plant and the feedback of a negative feedback control loop, respectively. The closed loop function $W(\mathrm{s})$ is:

$$W(\mathrm{s}) = \frac{\widehat{\vartheta}_{\mathrm{me}}(\mathrm{s})}{\vartheta_{\mathrm{me}}(\mathrm{s})} = \frac{R(\mathrm{s})P(\mathrm{s})}{1 + R(\mathrm{s})P(\mathrm{s})F(\mathrm{s})}. \tag{25}$$

Let $W^*(\mathrm{s})$ be the desired closed loop TF, the regulator can be designed as:

$$R(\mathrm{s}) = \frac{W^*(\mathrm{s})}{P(\mathrm{s})\left[1 - F(\mathrm{s})W^*(\mathrm{s})\right]}. \tag{26}$$

The DS method could lead to a no-proper TF of the regulator. The closed loop function must be selected carefully and in compliance with the analysed system. It is not seldom to get a regulator more complex than a simple proportional integral control. However, if $P(\mathrm{s})$ well describes the real system, the synthesised regulator allows to have the desired and accurate input-output behaviour. Finally, it is worth highlighting that the regulator obtained by the DS method is only able to accomplish an input-output relationship. Thus, the rejection capability can be verified only a-posteriori.

The observer loop schematic is reported in Figure 5, and the open loop TF is composed by (19) with an additional integrator to get the motor position from the estimated speed, namely:

$$P(\mathrm{s}) = \frac{L_\Delta U_h}{L_d L_q \omega_h \mathrm{s}} F^{\Sigma}_{\mathrm{HPF}}(s)F_{\mathrm{LPF}}(\mathrm{s}) = \frac{P^{\mathrm{new}}_{\mathrm{obs}}(\mathrm{s})}{\mathrm{s}}. \tag{27}$$

In order to obtain a feasible regulator, a second–order closed loop TF must be chosen, such as:

$$W^*(\mathrm{s}) = \frac{\omega_{\mathrm{obs}}^2}{\mathrm{s}^2 + 2\omega_{\mathrm{obs}}\xi_{\mathrm{obs}}\mathrm{s} + \omega_{\mathrm{obs}}^2} \tag{28}$$

where ω_{obs} is the desired bandwidth of the observer and $\xi_{\mathrm{obs}} = 1/\sqrt{2}$ is the critical damping factor which allows to have a $-3\,\mathrm{dB}$ gain at ω_{obs}. By substituting (27) and (28) in (26) and considering $F(s) = 1$, the design of the DS observer regulator is obtained in Laplace domain. The implementation in discrete time can be obtained by the well–known Tustin approximation. A third order TF in the z TF domain is obtained and its implementation requires only seven multiplications and seven additions. Figure 6 shows the synthesised controller with two desired closed–loop bandwidth. It has an almost constant frequency behaviour with a small ditch due to the $F^{\Sigma}_{\mathrm{HPF}}(\mathrm{s})$ sag and it lacks of integrators in the origin.

B. Internal Model Principle

The internal model principle states that a feedback system can completely reject a disturbance if the open loop TF includes its model [13], [14]. In a sensorless drive, the desired disturbance to be rejected is the actual position, see Figure 5, in steady-state condition which corresponds to a ramp–varying signal. In order to attain the control objective, the open loop TF must include the disturbance model, namely a double integrator. In order to obtain the position from the speed, an integrator is already present in the open loop transfer function as inferable from Figure 5. Then, the regulator can have only one additional integrator. An appropriate controller

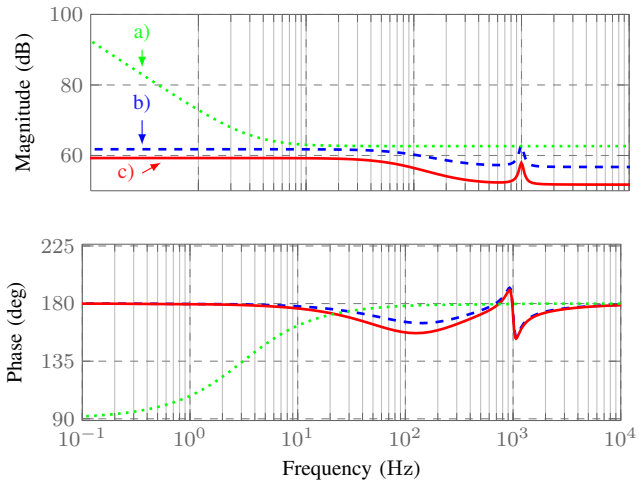

Fig. 6: Transfer function of the observer regulators: a) PI for a cross-over frequency of 60 Hz, b) DS with $\omega_{\text{obs}} = 80\,\text{Hz}$, c) DS with $\omega_{\text{obs}} = 60\,\text{Hz}$.

that satisfies the internal model principle is a proportional-integral (PI) controller that can be tuned imposing cross-over frequency and phase margin. The PI controller can completely reject the position disturbance, but its design cannot guarantee a fine control on the closed-loop roll-off frequency as in the direct synthesis method.

C. Comparison between observer regulators

The proposed controller design procedures aim at two different goals, i.e. to get an accurate control on the system bandwidth and the complete disturbance rejection. Two regulators obtained by the DS approach, with a desired closed-loop bandwidth of 60 Hz and 80 Hz, and a PI with cross–over frequency of 60 Hz and phase margin of 70 ° are depicted in Fig. 6. The 80 Hz PI controller is not feasible. The first important difference between the two methods is that the direct synthesis is always able to synthesise a feasible regulator, provided that a suitable desired closed loop TF is chosen. Moreover, the obtained closed–loop bandwidth coincides with the desired specifics. Indeed, a $-3\,\text{dB}$ closed–loop gain at 60 Hz is obtained by the DS regulator. On the other hand, the actual bandwidth obtained by the PI controller is about 85 Hz, i.e. almost 50% greater that the desired one.

The disturbance rejection capability of the controllers can be evaluated by using the *final value theorem*. The steady–state estimation error in response to a ramp varying disturbance can be computed as:

$$\widetilde{\vartheta}_{\text{me}}(+\infty) = \lim_{\text{s}\to 0} \text{s}U(\text{s})\frac{\widetilde{\vartheta}_{\text{me}}(\text{s})}{\vartheta_{\text{me}}(\text{s})} = \lim_{\text{s}\to 0}\frac{1}{s}\frac{\widetilde{\vartheta}_{\text{me}}(\text{s})}{\vartheta_{\text{me}}(\text{s})} \tag{29}$$

where $U(\text{s})$ is the input TF. The PI regulator with its integral part satisfy the requirement of the internal mode principle, and therefore it is able to fully reject the ramp-varying disturbance ($\widetilde{\vartheta}_{\text{me}}(+\infty) = 0$). Conversely, the DS regulator steady state error is:

$$\widetilde{\vartheta}_{\text{me}}(+\infty) = -\frac{2\xi_{\text{obs}}}{\omega_{\text{obs}}}\omega_{\text{me}} \tag{30}$$

TABLE I: Plate data of the motor under test

Parameter	Symbol	PMSM
Resistance	R	$2.726\,\Omega$
d-axis inductance	L_d	$26.5\,\text{mH}$
q-axis inductance	L_q	$114.7\,\text{mH}$
Permanent magnet	Λ_{mg}	$0.22\,\text{V s}$
Nominal current	I_N	$4.2\,\text{A}$
Nominal torque	T_{N}	$4.7\,\text{N m}$
Nominal speed	ω_{N}	$3000\,\text{rpm}$

TABLE II: Sensorless parameters

Parameter	Symbol	
Injection pulsation	ω_h	$2\pi 1\,000\,\text{rad/s}$
Injection magnitude	U_h	$60\,\text{V}$
F_{HPF} cutoff pulsation	ω_{H}	$2\pi\,100\,\text{rad/s}$
F_{LPF} cutoff pulsation	ω_{L}	$2\pi\,200\,\text{rad/s}$

which is proportional to the electromechanical speed ω_{me}. In order to decrease it, the damping factor could be reduced, but a resonance peak will appear in the closed loop observer TF. It is worth noting that $\xi_{\text{obs}} = 1/\sqrt{2}$ is the smallest damping factor which avoids peaks in the TF. To decrease $\widetilde{\vartheta}_{\text{me}}(+\infty)$, the only effective way is to increase the observer bandwidth, but at the price of a more disturbed position estimate.

V. Experimental results and discussion

The proposed estimator TF was verified throughout an extensive experimental stage. The tests were performed on an IPM motor, whose parameters are reported in Table I. The sensorless drive parameters are listed in Table II. The current controllers were designed to achieve a bandwidth of 100 Hz. The sampling frequency was set equal to the switching frequency at 10 kHz. The techniques were implemented on a dSpace MicroLabBox platform. Since the focus was on the design of the observer, the experimental AC drive made used of measured position and speed. So doing, the improvements of the design obtained by the proposed system model are not influenced by any other factor and the comparison with the conventional model is made easier.

In order to prove the effectiveness of the proposed estimator TF, three different tests were carried out. The first test was aimed at verifying the time response and the feasibility of the observers and it is reported in Section V-A. The goal of the second test was to identify the closed-loop frequency behaviour of the observer and it is described in Section V-B. Finally, the position tracking capability of the observer is verified with a real test case, and it is reported in Section V-C.

A. Observer time response and stability issues

Several controllers were designed to validate the proposed plant model and to compare the effects on the design of both DS and PI regulators. For the two observer models, i.e. (8) and (19), and for both DS and PI regulators, five designs with different control bandwidths were synthesised. The PIs were designed to achieve a phase margin of 70 °. Some preliminary experiments put in evidence that some combinations of required bandwidth and type of regulator

TABLE III: Stable observer combinations as function of the required bandwidth.

	10 Hz	30 Hz	50 Hz	100 Hz	150 Hz
DS + $P_{\text{obs}}^{\text{new}}(\text{s})$	✓	✓	✓	✓	✓
DS + $P_{\text{obs}}^{\text{past}}(\text{s})$				✓	✓
PI + $P_{\text{obs}}^{\text{new}}(\text{s})$	✓	✓	✓		
PI + $P_{\text{obs}}^{\text{past}}(\text{s})$			✓	✓	✓

were unstable. Table III reports all cases that exhibit a stable behaviour. Only the direct synthesis method coupled to the proposed model $P_{\text{obs}}^{\text{new}}(\text{s})$ is able to return a stable observer in the whole wide range of desired closed–loop bandwidths.

The results of Table III point out the controllers feasibility without showing any information on the dynamic behaviour of the obtained observers. To evaluate the real performance of a system, the time response to a step reference can be evaluated and Figure 7 depicts the observer responses to a $I_{h,q}^{*}$ step variation (see Figure 5). The observer behaviour can be estimated by evaluating the current transient. Each subfigure reports $I_{h,q}$ when a $I_{h,q}^{*}$ current step of $1\,\text{mA}$ is applied at time $5\,\text{ms}$. The step magnitude has to fulfil two opposing objectives, namely it has to be small because a small–signal analysis must be carried out to study a non-linear system but it has to be large enough to be measurable. It is worth noting that $I_{h,q}$ is the projection on the estimated *q*-axis of the current induced by the *d*–axis voltage injection. Therefore, $I_{h,q}$ is not a directly measured quantity. Actually, the injected high frequency voltage was $60\,\text{V}$ and the induced high frequency *d*-axis current was about $360\,\text{mA}$. A forced step of $1\,\text{mA}$ in the *q*-axis reference is a feasible way to investigate the closed loop behaviour of Fig. 5. In each subfigure, the desired step transient, namely the one corresponding to (28), is drawn. It is worth remembering that if the plant is well described via a TF, the DS output is a regulator that perfectly attains the desired behaviour. Therefore, if the measured $I_{h,q}$ is overlapped with the theoretical curve, it means that the system is well described.

All the step responses obtained with a regulator designed by the DS and the new TF (19) are in accordance with the theoretical ones, proving that (19) properly describes the estimator plant. System responses obtained with a DS controller synthesised with the wrong TF (8) deviate from the theoretical curves, becoming first oscillating and then unstable reducing the desired bandwidth. It is worth noting that (8) has a smaller static gain in the low frequency range than (19). If the desired closed–loop bandwidth is small, the regulator has to compensate the small plant gain. Since the real observer TF is (19), in the low range the resulting open loop TF gain becomes overblown, leading to instability. Finally, it is worth noting that PIs tuned with (19) returned a faster transient than the desired one, in accordance with the transfer function analysis carried out in Section IV-C.

B. Frequency identification

In Section V-A, the observer time behaviours designed with both existing and proposed model were studied and compared. In order to estimate the real frequency response of the position observer, i.e. the TF (25), the motor was forced to oscillate by means of an alternating torque produced by an active load directly connected to the motor shaft. The TF was obtained from the fundamental components of the measured position and the estimated one. Figure 8a reports the reference TF (25) in solid blue line, the actual TF obtained by the observer designed with the proposed model (red circles) and the TF relative to the observer based on the existing model (green diamonds). It is easy to recognise a close correspondence between the TF obtained by the new model and the designed reference (28). The same does not applied to the TF obtained with the conventional model that has a very different behaviour already from low frequencies. In all cases, the regulator in the observer was designed by the direct synthesis method and the desired closed–loop bandwidth was set at $80\,\text{Hz}$. The detail of the time response at $80\,\text{Hz}$ is also reported in Figure 8b. It is worth noting that the angular shift between the two signals is $93°$, very close to the theoretical value of $90°$. This experiments prove that a designed based on the proposed comprehensive model is fundamental to obtain a frequency response of the observer close to the reference one.

The slight difference between reference and measured TFs can be cancelled by replacing the critical damping factor by 0.82 in equation (28), while keeping constant the natural frequency $\omega_{\text{obs}} = 2\pi 80\,\text{rad/s}$. This can be explained by considering that in the real drive a higher damping factor than the desired one was expected due to dissipative effects. Anyway, the transfer function mismatch is really modest, so one can conclude that the plant description (19) can be considered exact.

C. Position tracking

A suitable experiment was designed to test the tracking ability of the position observer at zero or low motor speed. The proposed observer design by both PI and DS were first tested at zero motor speed and then at 0.1 (p.u.) motor speed, Fig. 9a. In both cases the load torque has been applied to the motor shaft (Fig. 9b). The performances are evaluated by mean of the estimation error $\widetilde{\vartheta}_{\text{me}}$ as shown in Figure 9c. The DS regulator was designed to get a closed-loop bandwidth of about $80\,\text{Hz}$ and a critical damping factor. The PI cross-over frequency and phase margin were selected as described in Section IV to get a similar closed-loop bandwidth, (it resulted of about $85\,\text{Hz}$). The static gain of the observer was kept constant by varying the parameters, that were stored in a look-up table as function of the stator currents.

At standstill, the two regulators have comparable performance since the position errors are very close to each other. The error is close to zero almost everywhere, showing excellent tracking capability. The error at full load is due to the cross–differential inductances, since the IPM motor slightly suffers of saturation and cross coupling among axis, as described in Section III-C. By computing the position error $\bar{\vartheta}$ due to the cross-inductances with the estimated ones at the rated load operating point, it is $\bar{\vartheta} = -0.09\,\text{rad}$ which is comparable to the obtained experimental error.

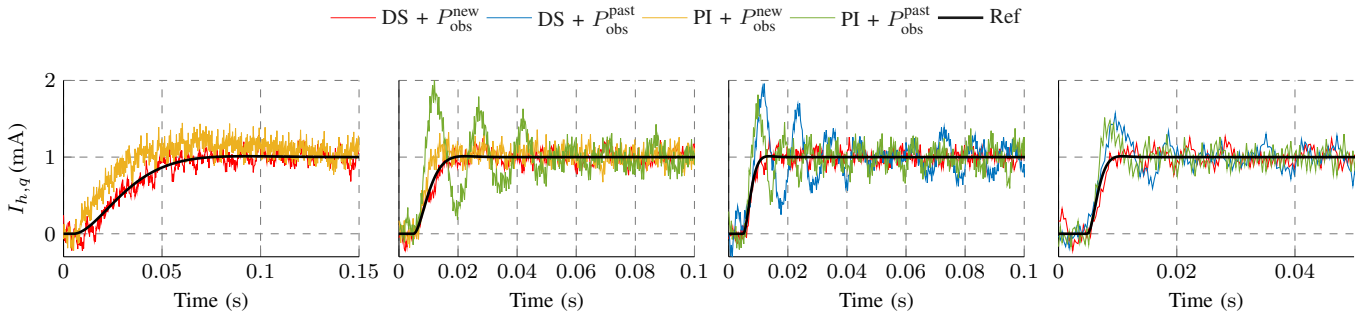

(a) Tuned @10 Hz (b) Tuned @50 Hz (c) Tuned @100 Hz (d) Tuned @150 Hz

Fig. 7: Step responses of all synthesizable regulators listed in Table III. Each subfigure depicts the observer response to a $I^*_{h,q}$ step variation. All the transients are collected according to the desired bandwidth. In each figure, the nominal response is shown as well.

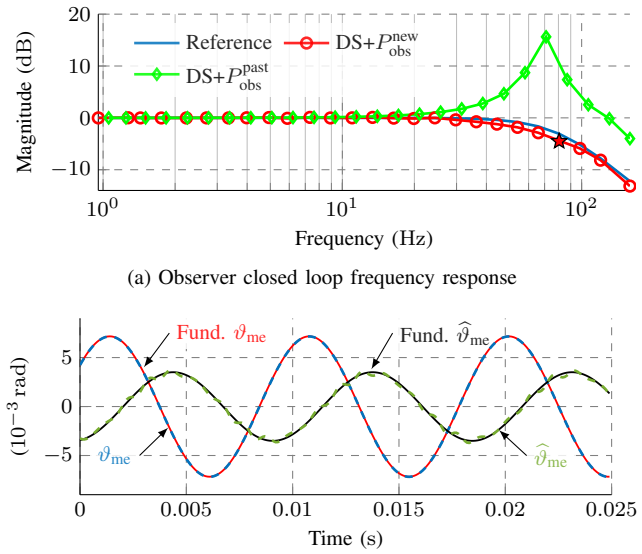

(a) Observer closed loop frequency response

(b) Observer time response @80 Hz, (★ in Figure 8a)

Fig. 8: Experimental closed loop frequency response of the observer (25).

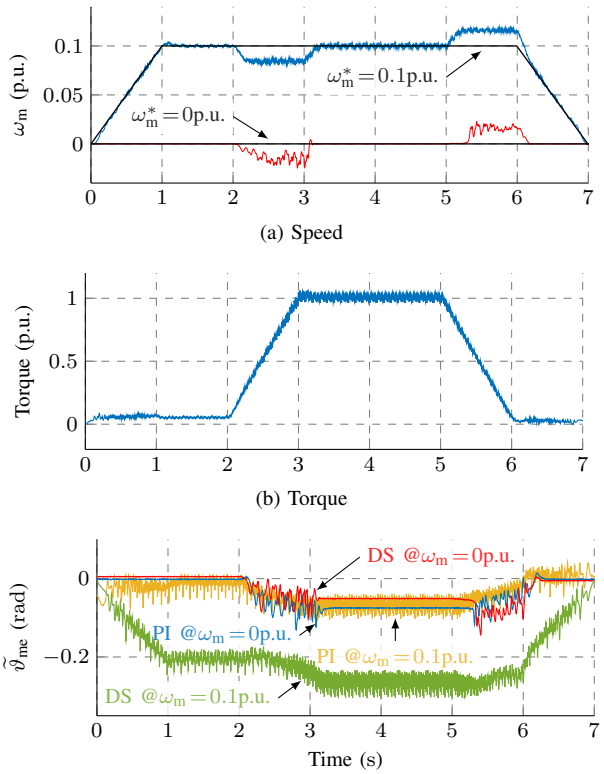

(a) Speed

(b) Torque

(c) Position error

Fig. 9: Speed, torque and position error of dynamic tests. Four tests are depicted with two different operating speeds and two regulators.

The observers performance deeply differ at non zero motor speed. The PI was able to fully reject the actual position disturbance, as motivated in Section IV-C. According to the related discussion, the DS controller showed a tracking error proportional to the electromechanical speed, as explained in Section IV-C. Evaluating (30) at no load condition, error of $\tilde{\vartheta}_{me}(+\infty) = -0.205\,\text{rad}$ was obtained, very close to the experimentally measured error of the test in Figure 9c. When the load was applied, the position error further increased of $\bar{\vartheta} = -0.09\,\text{rad}$.

VI. Conclusions

The paper reports a new transfer function description of the pulsating injection-based position observer. The modulation/demodulation theory has been exploited to derive the proper TF able to model the system. The new plant description differs from the classical formulation for a different high pass filter description due to the demodulation process. In order to experimentally verify the new TF, a regulator designed by means of the direct synthesis method is chosen since it allows to have a fine control on the closed–loop transfer function. The identified system well matches with the theoretical one, entailing the correctness of the proposed observer model.

A PI-based observer has been compared with one obtained by the DS controller, both tuned with the classical observer TF and the proposed one. A superior bandwidth control has been attained with the DS regulator, but the disturbance rejection incapability makes it unsuitable for a practical implementation.

The PI fully reject the ramp-varying position disturbance at the expense of less control over the achievable closed–loop bandwidth. Nevertheless, this flaw can be solved with an iterative tuned procedure exploiting the proposed sensorless model.

APPENDIX

Expanding the expression of $Y_5(\mathrm{s})$ (15) by using (14) and zeroing $U_\mathrm{q}(\mathrm{s})$ yields:

$$\begin{aligned} Y_5(\mathrm{s}) = \frac{j}{4}\Big[& U_\mathrm{d}(\mathrm{s})\left(G_\Sigma(\mathrm{s}-j\widetilde{\omega}_\mathrm{me}) - G_\Sigma(\mathrm{s}+j\widetilde{\omega}_\mathrm{me})\right)\dots \\ & - U_\mathrm{d}(\mathrm{s}+j2\widetilde{\omega}_\mathrm{me})G_\Delta(\mathrm{s}+j\widetilde{\omega}_\mathrm{me})\dots \\ & + U_\mathrm{d}(\mathrm{s}-j2\widetilde{\omega}_\mathrm{me})G_\Delta(\mathrm{s}-j\widetilde{\omega}_\mathrm{me})\Big] \end{aligned} \tag{31}$$

where $G_\Sigma(\mathrm{s}) = G_\mathrm{d}(\mathrm{s}) + G_\mathrm{q}(\mathrm{s})$ and $G_\Delta(\mathrm{s}) = G_\mathrm{d}(\mathrm{s}) - G_\mathrm{q}(\mathrm{s})$. When the observer is locked to the actual position of the motor, the estimation error is small and $\widetilde{\omega}_\mathrm{me} \approx 0$ then (31) can be approximated as:

$$\begin{aligned} Y_5(\mathrm{s}) = \frac{j}{4}\Big[& - U_\mathrm{d}(\mathrm{s}+j2\widetilde{\omega}_\mathrm{me})G_\Delta(\mathrm{s}+j\widetilde{\omega}_\mathrm{me})\dots \\ & + U_\mathrm{d}(\mathrm{s}-j2\widetilde{\omega}_\mathrm{me})G_\Delta(\mathrm{s}-j\widetilde{\omega}_\mathrm{me})\Big]. \end{aligned} \tag{32}$$

Now, replacing the equation (32) into (16) yields:

$$Y_8(\mathrm{s}) = \frac{F_\mathrm{LPF}(\mathrm{s})}{8}\left[F_\mathrm{HPF}(\mathrm{s}-j\omega_h)\sigma_1 - F_\mathrm{HPF}(\mathrm{s}+j\omega_h)\sigma_2\right] \tag{33}$$

where

$$\begin{aligned} \sigma_1 = & U_\mathrm{d}(\mathrm{s}-j(\omega_h+2\widetilde{\omega}_\mathrm{me}))G_\Delta(\mathrm{s}-j(\omega_h+\widetilde{\omega}_\mathrm{me})) \\ & - U_\mathrm{d}(\mathrm{s}+j(2\widetilde{\omega}_\mathrm{me}-\omega_h))G_\Delta(\mathrm{s}+j(\widetilde{\omega}_\mathrm{me}-\omega_h)) \\ \sigma_2 = & U_\mathrm{d}(\mathrm{s}+j(\omega_h-2\widetilde{\omega}_\mathrm{me}))G_\Delta(\mathrm{s}+j(\omega_h-\widetilde{\omega}_\mathrm{me})) \\ & - U_\mathrm{d}(\mathrm{s}+j(2\widetilde{\omega}_\mathrm{me}+\omega_h))G_\Delta(\mathrm{s}+j(\widetilde{\omega}_\mathrm{me}+\omega_h)). \end{aligned} \tag{34}$$

Neglecting the resistive contribution to the injection frequency, considering the injection pulsation much greater than $\widetilde{\omega}_\mathrm{me}$ and replacing to $U_\mathrm{d}(\mathrm{s})$ the Laplace transform of $\widehat{u}_{h,d}$, σ_1 can be written as follow:

$$\begin{aligned} \sigma_1 = \frac{2L_\Delta U_h}{L_d L_q \omega_h}\Bigg[& \frac{\omega_h}{(s-j(\omega_h-2\widetilde{\omega}_\mathrm{me}))^2+\omega_h^2}\dots \\ & - \frac{\omega_h}{(s-j(\omega_h+2\widetilde{\omega}_\mathrm{me}))^2+\omega_h^2}\Bigg]. \end{aligned} \tag{35}$$

Expression (35) can be rearranged to highlight that it is composed by three sinusoidal waves at the pulsations of $2\widetilde{\omega}_\mathrm{me}$, $2(\omega_h+\widetilde{\omega}_\mathrm{me})$ and $2(\omega_h-\widetilde{\omega}_\mathrm{me})$, namely:

$$\begin{aligned} \sigma_1 = \frac{2L_\Delta U_h}{L_d L_q \omega_h}\Bigg[& \frac{2\widetilde{\omega}_\mathrm{me}}{\mathrm{s}^2+4\widetilde{\omega}_\mathrm{me}^2} - \frac{(\omega_h+\widetilde{\omega}_\mathrm{me})+j0.5\mathrm{s}}{\mathrm{s}^2+4(\omega_h+\widetilde{\omega}_\mathrm{me})^2}\dots \\ & + \frac{(\omega_h-\widetilde{\omega}_\mathrm{me})+j0.5\mathrm{s}}{\mathrm{s}^2+4(\omega_h-\widetilde{\omega}_\mathrm{me})^2}\Bigg]. \end{aligned} \tag{36}$$

After filtering it with the low–pass filter $F_\mathrm{LPF}(\mathrm{s})$, the terms around twice the modulation frequency ω_h in (36) are suppressed. A similar procedure can be adopted for σ_2. Finally, noting that:

$$\mathcal{L}^{-1}\left(\frac{2\widetilde{\omega}_\mathrm{me}}{\mathrm{s}^2+4\widetilde{\omega}_\mathrm{me}^2}\right) = \sin(2\widetilde{\omega}_\mathrm{me}t) = \sin(2\widetilde{\vartheta}_\mathrm{me}) \tag{37}$$

and linearising it for small estimation error, expression (17) is obtained.

REFERENCES

[1] I. Boldea, M. C. Paicu, and G. Andreescu, "Active flux concept for motion-sensorless unified AC drives," *IEEE Trans. Ind. Electron.*, vol. 23, no. 5, pp. 2612–2618, 2008.

[2] Zhiqian Chen, M. Tomita, S. Doki, and S. Okuma, "An extended electromotive force model for sensorless control of interior permanent-magnet synchronous motors," *IEEE Trans. Ind. Electron.*, vol. 50, no. 2, pp. 288–295, 2003.

[3] V. Manzolini and S. Bolognani, "On the rotor position self-sensing capability of reluctance and ipm synchronous motors," *IEEE Trans. Ind. Appl.*, vol. 56, no. 4, pp. 3755–3766, 2020.

[4] Y. Kwon, J. Lee, and S. Sul, "Recent advances in sensorless drive of interior permanent-magnet motor based on pulsating signal injection," *IEEE Trans. Emerg. Sel. Topics Power Electron.*, pp. 1–1, 2020.

[5] M. W. Degner and R. D. Lorenz, "Using multiple saliencies for the estimation of flux, position, and velocity in AC machines," *IEEE Trans. Ind. Appl.*, vol. 34, no. 5, pp. 1097–1104, 1998.

[6] M. Berto, P. G. Carlet, V. Manzolini, and L. Alberti, "An effective ellipse fitting technique of the current response locus to rotating HF voltage injection in IPMSM for sensorless rotor position estimation," in *IECON 2018 - 44th Annual Conference of the IEEE Industrial Electronics Society*, 2018, pp. 391–396.

[7] T. C. Lin and Z. Q. Zhu, "Sensorless operation capability of surface-mounted permanent-magnet machine based on high-frequency signal injection methods," *IEEE Trans. Ind. Appl.*, vol. 51, no. 3, pp. 2161–2171, 2015.

[8] Ji-Hoon Jang, Seung-Ki Sul, Jung-Ik Ha, K. Ide, and M. Sawamura, "Sensorless drive of surface-mounted permanent-magnet motor by high-frequency signal injection based on magnetic saliency," *IEEE Trans. Ind. Appl.*, vol. 39, no. 4, pp. 1031–1039, 2003.

[9] V. Manzolini, M. Morandin, and S. Bolognani, "The crowded axis of the frequency: Optimal pole/zero allocation for a full speed sensorless synchronous motor drives," in *2016 IEEE Energy Conversion Congress and Exposition (ECCE)*, 2016, pp. 1–8.

[10] K. Lau, G. Goodwin, and R. M'Closkey, "Properties of modulated and demodulated systems with implications to feedback limitations," *Automatica*, vol. 41, no. 12, pp. 2123 – 2129, 2005. [Online]. Available: http://www.sciencedirect.com/science/article/pii/S000510980500275X

[11] A. Yousefi-Talouki, P. Pescetto, and G. Pellegrino, "Sensorless direct flux vector control of synchronous reluctance motors including standstill, MTPA, and flux weakening," *IEEE Trans. Ind. Appl.*, vol. 53, no. 4, pp. 3598–3608, 2017.

[12] R. Antonello, L. Ortombina, F. Tinazzi, and M. Zigliotto, "Online stator resistance tracking for reluctance and interior permanent magnet synchronous motors," *IEEE Trans. Ind. Appl.*, vol. 54, no. 4, pp. 3405–3414, 2018.

[13] G. Bengtsson, *Output Regulation and Internal Model: A Frequency Domain Approach*, ser. Research Reports TFRT-3134. Department of Automatic Control, Lund Institute of Technology (LTH), 1976.

[14] R. Antonello, L. Ortombina, F. Tinazzi, and M. Zigliotto, "Enhanced low-speed operations for sensorless anisotropic PM synchronous motor drives by a modified back-EMF observer," *IEEE Trans. Ind. Electron.*, vol. 65, no. 4, pp. 3069–3076, 2018.

Ludovico Ortombina (M' 19) received the M.S and Ph.D. degree in Mechatronic Engineering from the University of Padova, Italy, in 2015 and 2019, respectively. Since August 2020, he is a Researcher with the Department of Industrial Engineering, University of Padova. His research interests include parameter estimation techniques for synchronous motors, sensorless controls and predictive control.

Dario Pasqualotto received the B.S. and M.S (cum laude) degrees in Mechatronic engineering from the University of Padova, Vicenza, Italy, in 2016 and 2018, respectively. He is currently working toward the Ph.D. degree in mechatronics engineering with the Department of Management and Engineering. His main research interests include modelling, predictive maintenance and control techniques for ac motors.

Mauro Zigliotto Mauro Zigliotto (M '98, SM '18) is a native of Vicenza, Italy. He is full professor of Electrical Machines and Drives at University of Padova, Italy and head of the Electric Drives Laboratory in Vicenza, Italy. Advanced control strategies and self-commissioning for ac motors are Prof. Zigliotto's main research interests. He is the secretary of the IEEE IAS-IESPELS North Italy Joint Chapter.

Fabio Tinazzi Fabio Tinazzi (M '16) received the B.S. and M.S., Ph.D. degree in Mechatronic Engineering from University of Padova in 2008, 2011 and 2015 respectively. Since January 2021, he is a Researcher at the Department of Management and Engineering, University of Padova, Vicenza, Italy. His main research interests include sensorless control, predictive control and parameter estimation techniques for ac motors.